Equalizing Photoelectron Response Across Scintillators Employing Wavelength Shifting Fibers

Sebastian Seeds

A senior honors thesis submitted in partial
fulfillment for the Honors Physics
Bachelors of Arts Degree at the
University of Colorado
College of Arts and Sciences
November 2014

Thesis Advisor: Prof. Jamie Nagle

Thesis Committee Members:
Prof. John Cumalat - Dept. of Physics
Prof. Jamie Nagle - Dept. of Physics
Prof. Adam Norris - Dept. of Applied Mathematics

Abstract

The PHENIX project (Pioneering High Energy Nuclear Interaction eXperiment) is a relativistic heavy ion physics collaboration and detector which investigates the quark-gluon plasma. Essential to this project is a hadronic calorimeter which makes use of scintillator plates to measure incident particle energies. The subject of this thesis and the research it describes is in equalizing the response from detection events across a scintillation panel using silicon photomultipliers for use in an upgrade to the PHENIX hadronic calorimeter. This research includes a many step hardware and software process from data collection to data analysis, and is both a hardware and software methods project. During this process, several methods for categorizing and quantifying characteristic behavior of scintillator panels which rely upon optical fibers to communicate with silicon photomultipliers have been explored. These methods will be detailed in the thesis which follows. The essential theory supporting each step in the experiment will be explained as well as the findings of the experiment. As such, this research is also results oriented. Over the project, we have succeeded in modeling the photoelectron count across test scintillator panels and have observed consistency in this behavior.

Acknowledgments

Foremost, professor Jamie Nagle deserves my sincerest thanks. His insight throughout this project has provided it with direction and purpose, has enabled my efforts to be more efficient and rewarding, and has made my time spent in the high energy nuclear physics lab at the University of Colorado my most valuable experience at the University.

I would also like to thank the several people I work with in the lab; Shawn Beckman, Theo Kobleski, Kurt Hill, Andrew Adare, and Darren McGlinchey. All have been unerringly helpful throughout my research, but Shawn has been essential for my understanding of the experimental apparatus.

There are many others without whom I would never have been able to complete this thesis or perform the research it details. They are too numerous to account for here. I simply hope that they know how much I appreciate them.

Contents

1 Background 1

1.1 Experimental Context 1
1.2 Experimental Goals 3
1.3 Setup and Overview 5

2 Experimental Procedure 8

2.1 Stage One: Beta Delivery 8
  2.1.1 Stepper Program 8
  2.1.2 Light Insulation 10
  2.1.3 Mechanical Rails 11
  2.1.4 Radioactive Source 13
2.2 Stage Two: Data Acquisition 14
  2.2.1 Scintillator 14
  2.2.2 Wavelength Shifting Fiber Optic 17
  2.2.3 Silicon Photomultipliers 19
  2.2.4 Pre-Amps 20
  2.2.5 Comparison Circuit 21
  2.2.6 Oscilloscope, DAQ, and Data Storage 22
2.3 Stage Three: Data Analysis 23
  2.3.1 Calibration 23
  2.3.2 Analysis Function 24
  2.3.3 Basic Interpreter 28
  2.3.4 Temperature Monitor 29
2.4 Ancillary Hardware 29
  2.4.1 Vacuum Chamber 29
  2.4.2 Thermistor 30

3 Data and Results 32

3.1 Apparatus and Analysis 32
  3.1.1 Fiber Geometry and Photoelectron Response 32
  3.1.2 Fitting and Photoelectron Peaks 34
  3.1.3 Secondary Tests 36
3.2 Future Projections 37
3.3 Conclusions 38

Appendices 40

A Circuit Diagram **40**

1 Background

1.1 Experimental Context

A few microseconds after the big bang, the entire universe was in a state of free quarks and gluons called the quark-gluon plasma – with a temperature over a trillion Kelvin. We can re-create tiny droplets of this quark-gluon plasma with giant accelerators by colliding ultra-relativistic heavy nuclei and converting their kinetic energy into heat. In order to study the plasma, occasionally two quarks have a very large momentum transfer scatter. The quarks then race through the plasma leaving some of their energy behind. The quarks eventually escape the plasma and quickly hadronize - i.e. they form a spray of many confined hadron particles in a cone. In the PHENIX project, we want to measure the particles in that cone to figure out the details of the high energy quark interactions with the plasma [2].

Thus we want to measure the energy of these individual particles accurately, then add them together into the jet that came from the quark. The proposed hadronic calorimeter can measure the energy of these individual particles. There are interleaved layers of steel to force the particles to interact and shower into even more particles, and then scintillator plates that measure the charged particles in this shower from the steel. The number of these final charged particles is roughly proportional to the energy of the incident particle on the hadronic calorimeter. We want to count these particles with even weight - so it is bad if a particle hitting one part of the scintillator gives more signal compared with a particle hitting another part of the scintillator. The initial goal of this experiment is to characterize any such differences, and then hopefully mitigate them.

To this end, many methods have been explored to quantify various physical characteristics of resultant particles after collision events. Many of these have enabled us to understand what particles are made of and how they behave in high energy contexts.

Work in high energy physics undertaken for this thesis and the research it describes is in conjunction with Brookhaven National Labs and the Relativistic Heavy Ion Collider (RHIC) in New York for the proposed sPHENIX upgrade to the PHENIX project [2]. The PHENIX project is the Pioneering High Energy Nuclear Interaction eXperiment which is located at RHIC. Specifically, the particle collider at RHIC explores conditions which likely existed immediately after the big bang. This is achieved with RHIC through many controlled particle collisions. The Nagle group at the University of Colorado Boulder works along with the larger PHENIX collaboration investigating the quark-gluon plasma.

One particular method for detecting the particle constituents of quark jets is through scintillation. At RHIC, the hadronic calorimeter (HCAL) and the electromagnetic calorimeter (EMCAL) both rely on this phenomena. In this process, a small flash of light is produced by a fluorescing material suspended in a polymer matrix by a particle which passes through it [6]. Scintillating plates are employed to detect some of the scattered remains of particle collisions, namely electrons and photons. Traditionally, photomultiplier tubes (PMTs) have been used to convert scintillated light into an electrical signal for further analysis. These PMTs are characteristically positioned next to a scintillator plate such that scintillated light enters a forward aperture. Due to high voltages across plates within the photomultiplier, this induces an avalanching effect of photoelectrons (PEs) via the photoelectric effect, wherein a small amount of incident light can result in a measurable voltage out of the PMT [7].

PMTs have certain drawbacks. Foremost among them is the skewing effect of latent magnetic fields on electrons within the device. When a PMT is placed in such a field, a magnetic field will cause any avalanching electrons to accelerate. This effect is dynamic, and often not consistent enough to correct for in the voltage signal out of the PMT. As such, PMTs aren't especially effective for the PHENIX project.

Responding to this issue, silicon photomultipliers (SiPMs) have seen use as an alternative. While the functionality of a SiPM is similar to that of traditional PMTs, such a photomultiplier is much smaller and often optically coupled to a fiber optic cable which can run through a scintillator panel. Due to their compact design, SiPMs are significantly less affected by latent magnetic fields [5]. This accounts for their potential strength over PMTs.

This said, SiPMs present challenges of their own. Because, for application at RHIC, SiPMs must be optically coupled to a fiber optic to function efficiently, they experience fluctuations in PE response. This phenomena is the result of a detection event's proximity to the fiber optic cable; those scintillation events which occur closer to the cable result in more light reaching the SiPM than those which occur farther away (Figure 1).

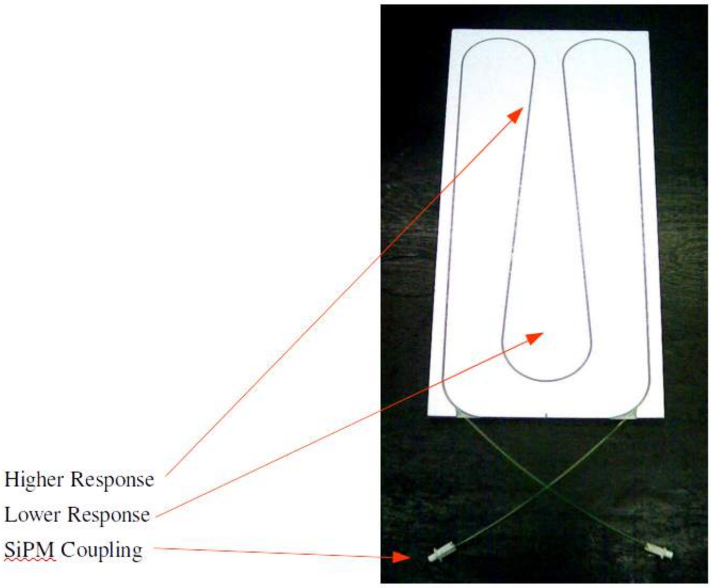

Figure 1: Light Yield Differential

This picture shows the expected and observed light yield differential across a typical scintillator plate. Because the HCAL fundamentally needs to measure differences in incident particle energies, it can benefit from excluding differences in energy due to incident particle location on the scintillator plate. Operationally, this might be accomplished with an experimental cut, preferentially removing all functional dependence of energy measurement as a function of distance from an optical fiber. This kind of cut might only be performed with accurate modeling of light attenuation across relevant scintillators as a function of distance alone.

1.2 Experimental Goals

The central goals of this experiment are twofold. Foremost, the goal of the experiment is to characterize the light yield response as a function of event distance from an embedded wavelength shifting (WLS) fiber over test scintillator panels reading out to optically coupled SiPMs. The optical fibers used in this experiment are wavelength shifting for reasons detailed in section 2.2. In order to obtain a quantified model for this, a Strontium-90 beta radiation source is positioned at controlled locations using a system of mechanical rails above a scintillator plate. The characterization of PE yield as a function of distance from a WLS fiber can be quantified by allowing for a consistent number of coincidence events at each computer designated location above the scintillator plate. Each coincidence event can be interpreted as an energy measurement and averaged into the total number of interpreted coincidence events at each location. Repeating this process enables, in whole or in part, a characterization of energy measurement across a scintillator panel as a function of location of energy deposition event. A detailed description of this experimental apparatus, hardware and software, follows in section 2.

Addressing this issue empirically will inform adequate experimental response towards optimization of the scintillator panel. The second major goal of the experiment is to produce a method for equalizing PE response for similar events across the scintillator plate. An example of expected PE response relative to a simplified flat geometry from a single straight fiber can be found in Figure 2. There are many other factors which influence the PE response, however, and the observed response differs from this model. Section 3.2 deals with these results. The two central methods which have been explored are particular wrappings of the scintillator plate, one of mylar and the other black paper, and preferential selection of fiber geometry through the scintillator. This thesis focuses on the latter method, but both are potentially viable. Success in optimizing fiber-optic lined scintillator plates here could allow for more general application in the HCAL at RHIC and elsewhere.

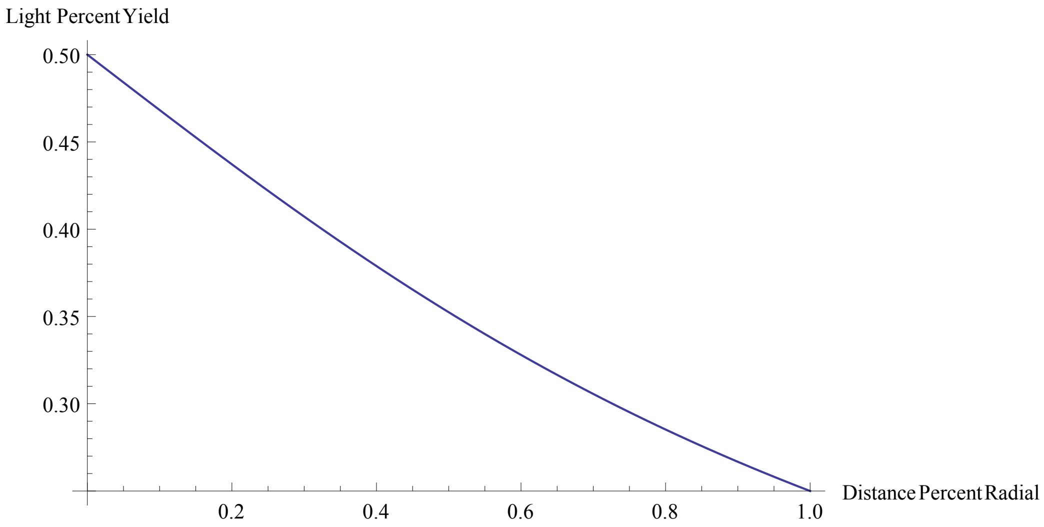

Figure 2: Simple Light Yield Model

Several factors exist which cause these goals to be difficult to attain. Noise from ambient light, cosmic rays, and crosstalk between hardware components all contribute to produce low PE peaks which must be distinguished from the principle data [5]. Penetration depth limits of the beta radiation from Strontium-90 prevent certain kinds of deliberate attenuation techniques designed to equalize response via wrapping. Functional dependence on distance as determined in the experiment indicate that early ideas for optimization need refinement. A detailed discussion of these issues can be found in section 3.

1.3 Setup and Overview

The experiment consists of three stages. The first stage, Beta Delivery, has both a hardware and software component. Computer controls from the data acquisition system (DAQ) direct the movements of a brass collimater which holds the Strontium-90 source vis a vis a mechanical track. On the software end, the computer controls consist of a widget program used to actuate the motors integral to the track system and C++ code designed to affect this actuation. On the hardware end, the Strontium-90 source is transported via mechanical rails which respond to the aforementioned motors. The hardware apparatus for this stage and the next are built within a black box in order to remove all significant ambient light sources in the ultraviolet and visible range of electromagnetic spectra for reasons detailed in section 2. While the black box and its architecture is essential for both stage one and stage two, it's been grouped into stage one for simplicity. The second stage, Data Acquisition, is largely hardware, but is integrated into the software detailed in stage one on the back end. This stage consists of several pieces of hardware. A milled scintillator plate with a WLS fiber running through it is attached to two SiPMs with one optically coupled to each end of the WLS fiber. From the SiPMs, a voltage pulse is amplified and shaped in two pre-amps which export their signals to a discriminator and to an oscilloscope. The discriminator triggers on coincidence between the two signals and is tuned to eliminate low voltage noise. The resulting trigger signal is sent to an oscilloscope such that it draws relevant data from the raw data inputted from the SiPMs. This final signal is processed on the oscilloscope for viewing and transfer to the DAQ. The final pulse is then stored in a file on the DAQ which corresponds to the position of the radioactive source. Stage three, Data Analysis, is purely software and consists of an analyzer program which integrates the many pulses stored per position of the source. These integrated values (in $V * s$) are averaged over the determined amount of pulses (ranging between 500 to 1000 events). These averaged values are fit to a calibrated Poisson distribution which correlates the averaged integrated pulse data to PE counts per location. This PE data is then binned to a histogram for interpretation.

Section 2 is a more detailed description of these components outlined in the stages described above. It is essentially an input/output model of each stage of the experiment with an overview of each component by subsection. Figure 3 is a block diagram of the experiment as a whole. Section 2 will proceed from beta delivery to data acquisition to data analysis. All hardware components will include a functional description and, where appropriate, an explanation of theory. For brevity, only a functional description of the software used will be given in section 2.

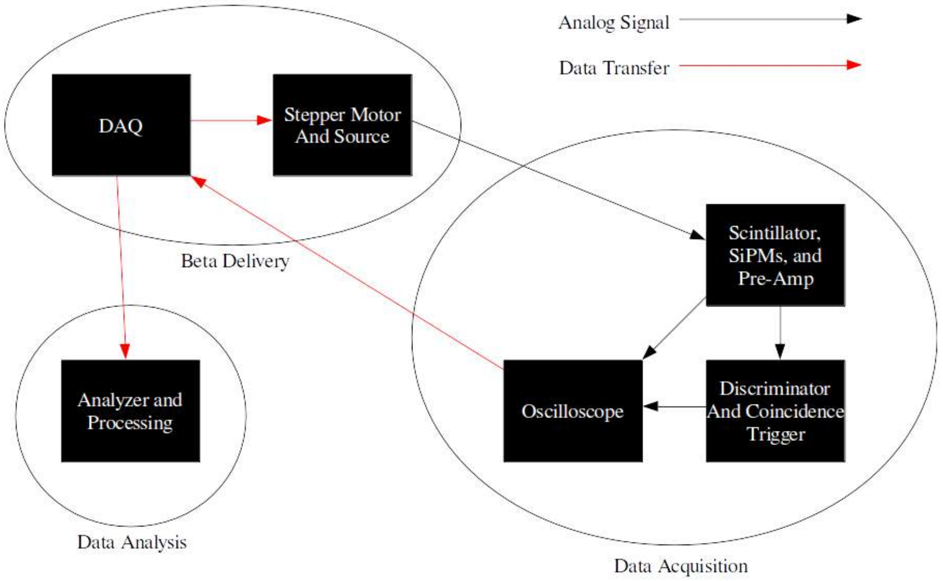

Figure 3: Block Diagram of Experiment

2 Experimental Procedure

2.1 Stage One: Beta Delivery

The beta delivery stage of the experiment includes both software and hardware and details the methods used in the experiment to deliver beta radiation to test scintillator panels. This delivery is controlled digitally, but actuated mechanically.

2.1.1 Stepper Program

Because the process of data acquisition often takes 2-3 days, this project is automated throughout. As such, actual data collection starts and ends with code located on the DAQ. In order to automate control of the stepper motor for use positioning the radioactive source (discussed in later subsections), a corresponding widget program must be employed along with a simple code operated from the terminal to instruct it. The stepper motors operate via a two dimensional position metric, quite simply X and Y. Each motor can be operated directly with the widget, a self contained program and generated user interface (GUI), or by input to the command line. The GUI is crude; it allows controlled movement over each motor with a sliding bar without ability to modify position steps by numeric value. This fact along with its need for human manipulation renders the GUI control method useful only for re-zeroing the positions of each carriage on its rail.

The command line method for manipulation is more precise and less demanding. Each X and Y axis length movement step of the source on its corresponding rail can be precisely set and looped over. Further, this movement can be facilitated contingently and set to proceed only after a determined amount of data collected from the oscilloscope. This allows for the final stage of data acquisition to feed back into the first, fully automating the process. The final stage of this section will tie back into this stage and vindicate this point.

Practically, this automation results in single pass movements of the radioactive source over the scintillator. In order to simplify descriptions, a nomenclature was developed to describe these scans. Looping over the X-axis first, with a nested loop over the Y-axis contained within, results in an N pass. Conversely, looping over the Y-axis first, with a nested loop over the X-axis within, results in a Z pass. The purpose for different scanning methods is to increase the robustness of our results. Figure 4 demonstrates this practical effect. Modification of the X and Y step length and step totals directly controls the total length of each pass actuated by a Velmex screw drive and the space between source locations [4]. The error in each space controlled by stepper movement is on the order of μm. This effectively controls the potential resolution of the final data product.

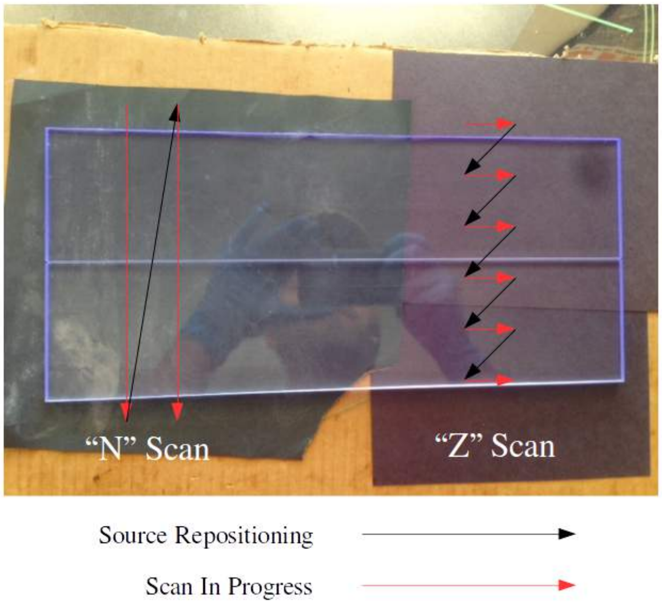

Figure 4: Z and N Scans

The control over the widget and corresponding stepper motors is automated via a C++ macro written for this purpose in Microsoft Visual C++. Some commented lines of code are periodically switched in where others uncommented are manually switched out to alternate between N and Z scans, to control the step length, and to control scan area. In this way, the code is manually altered between data sets to direct data collection towards different experimental goals.

The stepper controls on the DAQ are connected directly to the stepper motors via USB which first pass through the sidewall of an apparatus designed to insulate the experiment from ambient light. This apparatus is the subject of the next section.

2.1.2 Light Insulation

The singular method for insulating the radiation source and scintillator in the experiment is a wooden box of dimensions 86 × 86 × 124 cm. The box has been painted black and securely attached to a work bench for stability. Two apertures exist in the box. The first is on one of the small sidewalls and is designed for the passage of cables. This aperture has a small interim pocket such that cables to and from the interior might pass in and out of the box without compromising the light insulation the box provides. The second is on one of the large sidewalls, and consists of the entire sidewall panel. This aperture allows for manipulation of the contents of the box and is attached via three hinges which reside at the bottom of the aperture. The box is complete with two securing fasteners at the top of the aperture and a lock. Figure 5 depicts the apparatus.

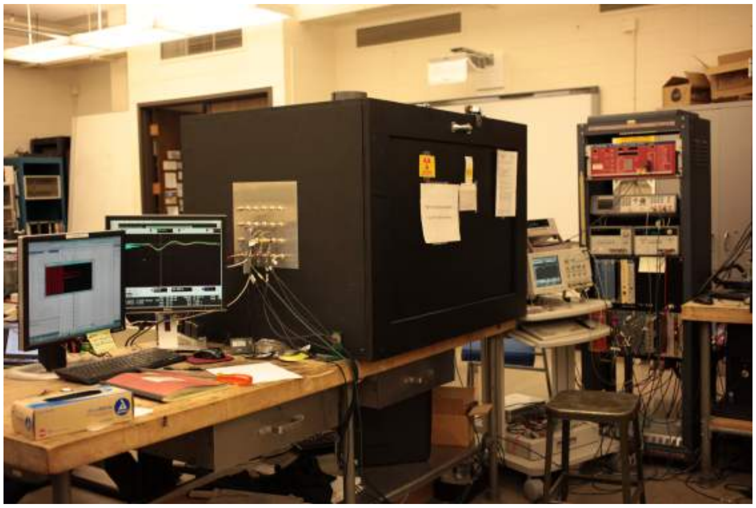

Figure 5: Exterior of Test Stand

It is possible to collect data from traditional photomultiplier tubes (PMTs) within the apparatus. As such, high voltage sources might be employed to generate sufficient voltage within a PMT inside the box for operation. In order to prevent damage to the PMT due to premature opening of the apparatus (and the resulting overload of current from the integral photoelectric response from the PMT), a safety voltage cutoff has been installed on the locking plates which complete a safety circuit with a separate high voltage source. If the box is not shut, the high voltage source will not supply voltage to the experiment.

The interior of the box is also painted black to minimize the effects of internal reflection where they exist. A light shielded vent exists in the top of the box to approximate thermal equilibrium with the exterior of the box, and several adjustable T-slotted aluminum pipes are positioned throughout. These pipes provide the structural means to construct platforms for scintillator panels and to attach screw drives with corresponding stepper motors. Figure 6 depicts this section of the apparatus.

Figure 6: Box Interior with Platform

2.1.3 Mechanical Rails

The Velmex screw drive and rail system employed for transporting the radiation source consists of two interlocking linear actuators, one corresponding to X motion as directed by the widget on the DAQ, and the other corresponding to Y motion. Each stepper motor controls a linear actuator which rotates a long screw, where each full rotation is a step as controlled by the widget [4]. The rail corresponding to the Y-axis is attached to the rail corresponding to the X-axis, such that one step on X moves the entire stepper assembly which controls Y by one step. Each step is on the order of 10 μm, with an error on the order of μm [4]. Particular to stepper motors is the fact that this error doesn't add between steps; it applies to each rotation of the screw independently. This means that any desired position will exhibit an error on the order of μm. The radiation source and collimator is attached to the Y rail and positioned with the screw which runs through it. In this way, both the X-axis and Y-axis positions of the radioactive source can be positioned with the stepper motors with excellent accuracy.

The top rail is securely attached to the top of the box. This both ensures a static zero for the radiation source and positions the source above such that scintillators might be tested beneath. Figure 7 depicts the mechanical rail section of the apparatus.

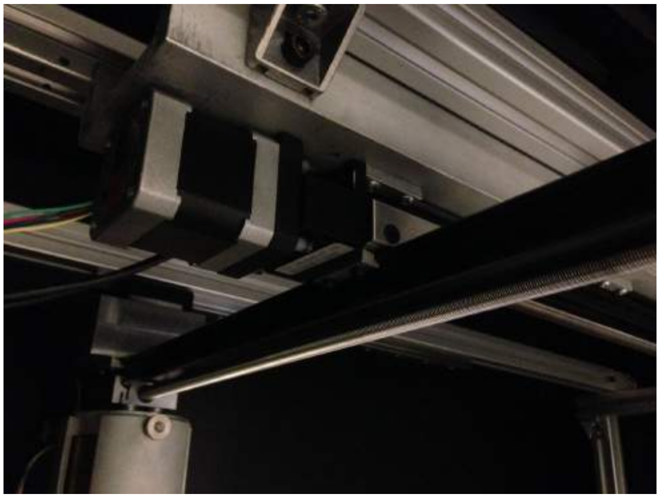

Figure 7: Rail System with Stepper Control

Each stepper motor operates on DC voltage and rotates a gear through its corresponding linear actuator with a series of electromagnets. The electromagnets surround the gear and are turned on in a rotational sequence [4]. This operation causes the teeth of the gear to align with the magnet which is on, causing overall rotation with precise digital steps issued by the DAQ. This gear then actuates a screw in its corresponding rail. The error on each step's movement along the rail is negligible for the experiment. The precision of this instrument is essential for consistent positioning of the radiation source. This ensures that the final data product is not distorted by position.

2.1.4 Radioactive Source

The radioactive sample used in this experiment to produce a consistent source of radiation is Strontium-90. This isotope of Strontium decays through beta emission into Yttrium-90, with a beta decay energy of about 0.55 MeV and a half life of 28 years. This Yttrium-90 decays further through beta emission into Zirconium-90 with beta decay energy of about 2.28 MeV and a half life of 64 hours [8]. These decays produce electrons with a spectrum of energies emitted from the radioactive source. The electrons emitted from this source cause scintillation in sample scintillator plates placed beneath it. This beta emission source simulates scintillation events from showering hadrons in the HCAL at RHIC.

The Strontium-90 source is contained in a solid brass cylinder, with a 1 mm diameter aperture milled through the bottom. This collimator shields the rest of the apparatus and experiment from the beta radiation emitted from the sample, but directs a stream of electrons down directly from the source. The brass collimator is attached to the Y-axis rail of the mechanical rail apparatus component and is positioned such that a stream of 0.55 MeV electrons can pass into a scintillating plate laid flat on an internal horizontal platform at normal incidence. Refer to Figure 8 for a picture of the radiation source. As controlled by the mechanical rail system by way of the DAQ unit, the Strontium-90 completes the beta delivery section of the experiment.

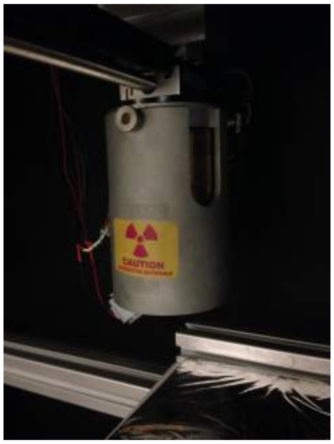

Figure 8: Strontium-90 Radiation Source

2.2 Stage Two: Data Acquisition

The data acquisition stage takes the light generated by beta radiation incident to a scintillator and processes it into a digital package for analysis. This stage is hardware oriented, including both analog and digital circuitry.

2.2.1 Scintillator

The event detectors used in this experiment are plastic organic scintillator plates. A scintillator is a substance which absorbs energy from incoming particle radiation and emits the energy deposited in the scintillator by such an event in the form of light. This emission is called florescence and the whole process is called scintillation.

The mechanism for scintillation in an organic scintillator such as the one used in this experiment begins with the excitation of electrons in the S00 state (or the lowest vibrational state of the ground electronic state) into an excited state. This energy is absorbed from the kinetic energy of passing charged particles. In order to maintain thermal equilibrium with its neighbors, higher vibrational modes of each electron excited into the S1N ($N = 1, 2, 3$) create a population of of excited molecules in the S10 state by dispersing their vibrational energies. After some characteristic decay time τ_f (particular to the scintillating molecule) the an electron in the excited S10 state decays back into a vibrational ground state denoted by S0N ($N = 1, 2, 3$) and fluoresces. The intensity of this florescence is given by:

$$I = I_0 e^{t/\tau_f}$$

which gives rise to a light pulse in very fast scintillators given by:

$$N = \alpha e^{t/\tau_f} + \beta e^{t/\tau_s}$$

where τ_s is the characteristic time for populating optical levels of electrons in the scintillator and N is the number of photons emitted. A typical for τ_s is 0.5 ns and a typical value for τ_f is 2 ns in very fast scintillators such as the ones tested in this experiment [10]. The final light versus time profile observed ends up being a distribution given by:

$$I/I_0 = f(t)e^{-t/\tau_f}$$

Here $f(t)$ is a Gaussian distribution function [10]. Figure 9 illustrates the excitation and emission typical for scintillation [10].

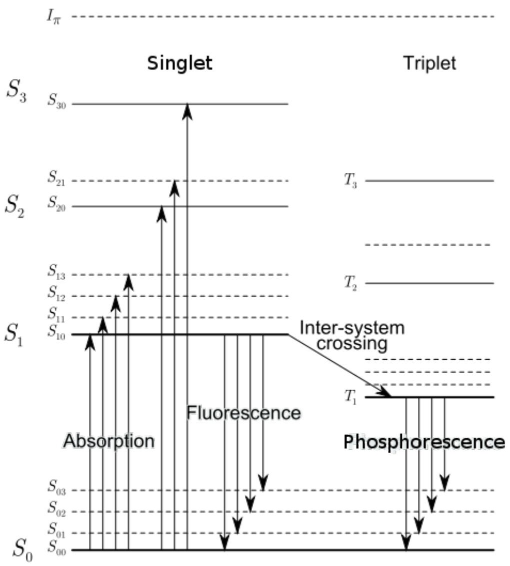

Figure 9: Electron Excitation and Emission

Because the mechanism for florescence is dependent upon vibrational fine structure of electronic transitions, the intensity of its response can be dependent upon changes in ambient temperature levels. This dependence is due to the thermodynamic affect on vibrational fine structure where higher temperatures result in higher fluorescence from a scintillator. To control for this, and the larger affect temperature has on SiPMs in the experiment, a thermistor has been installed in the light insulating box. This is discussed in more detail in section 3.13.

Light fluoresced from organic scintillators radiates in the ultraviolet, making its detection less efficient for SiPMs. For this reason, WLS fibers (as opposed to simple fiber optics) are employed to shift the wavelength of incoming light into a more readable range for the photomultiplier [1]. For the SiPMs in this experiment, the peak sensitivities are between 400 and 500 nm, in the visible spectrum [3]. Both WLS fibers and SiPMs will be discussed later in this section.

The scintillators employed in this experiment have been polished to ensure even surfaces. This maximizes total internal reflection from energy deposition events.

Several similar Uniplast scintillators have been used with this experimental apparatus, each with different fiber layouts [13]. The two layouts used to draw the conclusions here are simple ones. Figure 10 and Figure 11 depict these layouts. In the first, two grooves are milled 1 mm wide and 3 mm deep into the plate, one positioned in the center of the scintillator lengthwise, and the other 50 mm from the wide end width wise. In the second, one groove is milled 1 mm wide and 3 mm deep through the center of the plate. The particular dimensions of these plates are 33.0 × 15.3 cm. A WLS fiber is set into a groove with optical grease for layout 1 or epoxied into the groove for layout 2.

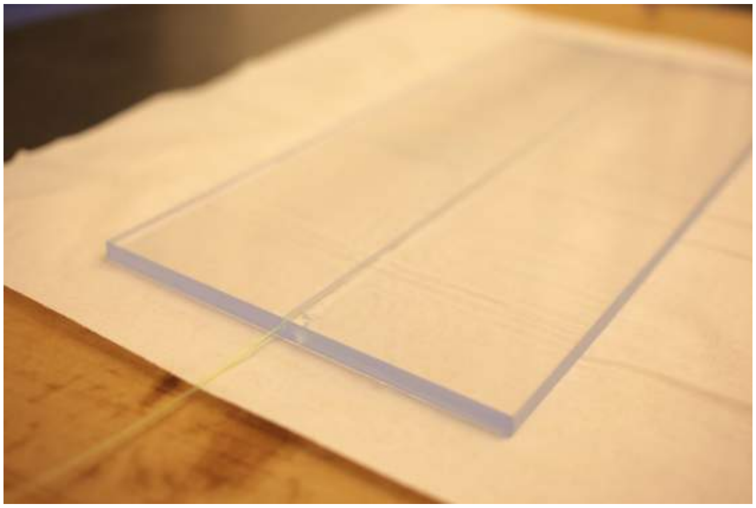

Figure 10: Scintillator Panel with Fiber at Middle

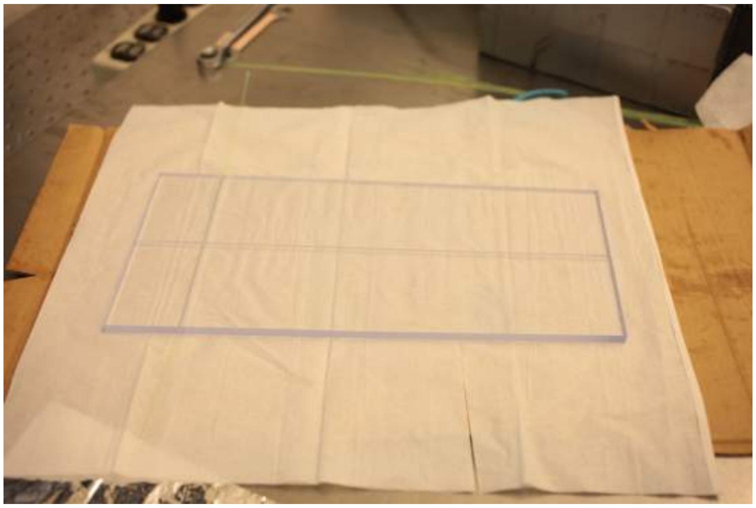

Figure 11: Scintillator Panel with Fiber at End

Several factors inherent to the scintillator influence the final data product. For example, the geometry of the scintillator enables internal reflection to be a factor in light yield from the SiPM. Energy deposition depth plays a role along with deposition distance from the WLS fiber as well. Many of these variables result in similar PE response regardless of position on the panel. As such, their effects average out and can be separated from (or don't influence) the primary signal generated by excitation events.

In order to obtain greater light yield from the scintillators in this experiment, each has been wrapped in aluminized mylar to encourage total internal reflection. This higher light yield results in elevation of meaningful fluorescence events above a set discriminated background around 1-2 PEs at the SiPM.

Similar scintillator plates to those tested in this experiment are used in the hadronic calorimeter at RHIC [13]. Investigation into the response and properties of scintillator plates, with a focus on equalizing response across ones that employ fiber optics, is the central focus of this research.

2.2.2 Wavelength Shifting Fiber Optic

Wavelength shifting fibers are themselves scintillators. When light of higher energy enters the fiber, an isotropic scintillation occurs where photons of lower energy are fluoresced. The process for this scintillation is similar to that described in section 2.21; incoming light is absorbed by electrons which excite them into higher energy states, some vibrational. These vibrational states even out over a population over some characteristic time interval, and decay back to their ground states over another characteristic time interval emitting photons of a characteristic wavelength. Some of this emitted light escapes back into the scintillator panel, but much of it is totally internally reflected. This results in an even signal at both eventual ends of the fiber from the internally reflected light.

Kuraray multiclad fibers with diameters of 1.2 mm are used in the experiment for their higher trapping efficiency over their single-clad alternatives. The core of the fiber is made of polystyrene followed by a sheath (or clad) of acrylic followed by a second clad of fluorinated-polymer [11]. Each clad improves the angle for internal reflection, redirecting light that would have escaped back into the fiber for collection at the end. This results in a higher trapping efficiency and improves the overall light yield per excitation event in the scintillator.

In addition to condensing the light output into a smaller cross sectional area (the end of the fiber), the WLS fibers also wavelength match for the SiPM optically coupled to the end [14]. The scintillator plate fluoresces in the ultraviolet spectrum, but the SiPM is most efficient in the visible spectrum. As such, WLS fibers laid into the plate shift the light from an excitation event down in frequency which improves the detection capability of the SiPM.

Each fiber is optically coupled to the scintillator which it is laid into using either optical grease or epoxy. One of the secondary objectives of this experiment has been to test the relative efficiency of optical grease versus epoxy for the purposes of light yield. This is discussed more in section 3.1. Optical coupling matches the index of refraction for the scintillator plate and the fiber such that incoming light is less easily reflected away from the fiber. Similar to the extra clad in the fiber, this increases the overall light yield per excitation event in the scintillator panel [2].

Due to the isotropic nature of the light scintillated in the fiber, each excitation event translated into the fiber can be read out of both ends of it. This enables triggering on coincidence of light entering the two separate SiPMs.

2.2.3 Silicon Photomultipliers

The silicon photomultiplier is arguably the most important piece of technology in the experiment. It is an array of roughly 1000 microscopic avalanche photodiodes (APDs) set in a common silicon base [9]. By applying a 71 V potential in the reverse bias direction over the SiPM, each APD in its array operates in reverse bias just outside of the breakdown voltage limit (65 V) [9]. This ensures that the SiPM is operating in Geiger mode and can give an appreciable signal from even one photon incident to the surface of the SiPM. The precise SiPM used in this experiment is Hamamatsu brand number S10362-11-0550C [9].

When a photon enters a reverse biased APD, a current is generated through impact ionization. In this process, the energy from an incident photon is consumed to free an electron from its valence band and promote it to the conduction band. Due to a large potential, this free electron is accelerated and periodically gives some of its energy to promote other electrons to the conduction band. This process is similar across all freed electrons and results in an electron avalanche which effectively maps an incident photon to a reasonably distinct measurable signal out of the APD. When a critical current is produced, a quenching resistor external to the APD reduces the voltage across the APD and ceases the avalanche [9]. The response rate for this process is on the order of picoseconds, which is important for the comparison circuit discussed in section 2.25.

The purpose for the array of similar APDs is to allow for multiple simultaneous detections of incident photons. This is accomplished through the SiPM's analog construction. Each of the APDs is connected in parallel such that multiple reasonably distinct photon signal amplitudes are independent of one another and add discretely. With this in mind, it is possible to see discrete peaks of PEs in a plot of events versus voltage out [9]. See figure 12 for an illustration of this effect which will be important for later discussion about calibration in section 2.3. Crosstalk between each APD, where electrons emitted from APDs are picked up by adjacent APDs, is minimized by constructed barriers between APDs in the array [9].

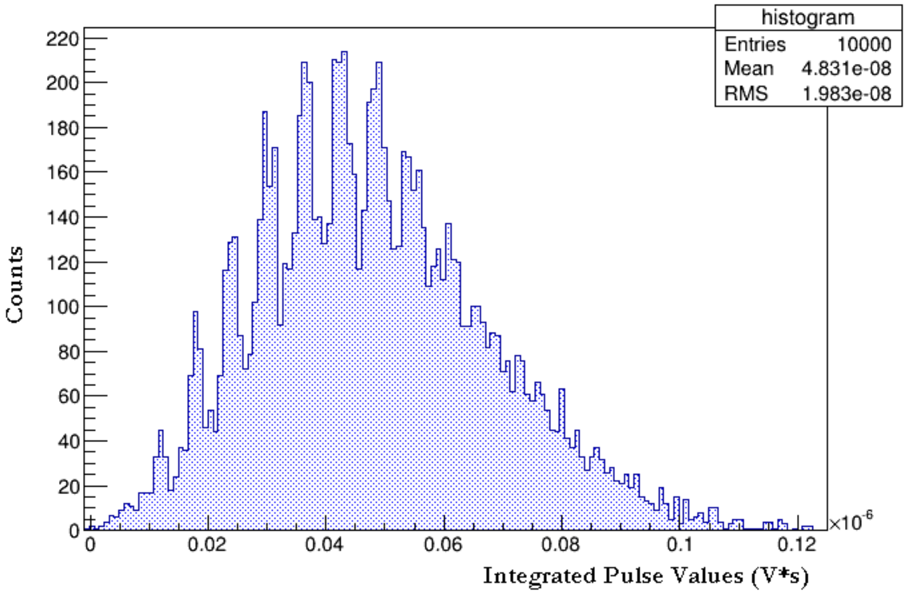

Figure 12: Calibration Histogram

The primary source of temperature dependence in the experiment comes from the SiPM. Ambient thermal variations can, in principle, cause significant scaling of the output signal [9]. As a control for this, temperature readings are taken from inside the box to be correlated to scaled signal differentials for scan histograms which display significant PE deviation. The results of this analysis can be found in section 3.1.

The SiPM has a peak wavelength sensitivity between 400 and 500 nm, somewhat above that of the peak emission wavelength of scintillator. The Kuraray fibers used in the experiment match this wavelength, as discussed earlier. The SiPM has a gain of roughly 105, but still needs further processing [9]. Toward this end, the current produced by each SiPM is fed into a pre-amp.

2.2.4 Pre-Amps

In order to obtain a uniform voltage pulse corresponding to PE events at the SiPM, a simple amplification circuit was constructed. This circuit has two primary effects. First, it takes a variable current in and outputs an amplified voltage signal pulse out. The gain of this amplification is adjusted to be 100. Second, the circuit takes a bias voltage and shapes an inverted pulse for later processing. This bias voltage is supplied from a separate Agilent voltage source kept at 6 V and 0.030 A. This is the final analog data product of the circuit, which it sends out to a splitter which then sends the signal to a comparison circuit and an oscilloscope. Figure 13 depicts a pulse from a photon detection event at the SiPM.

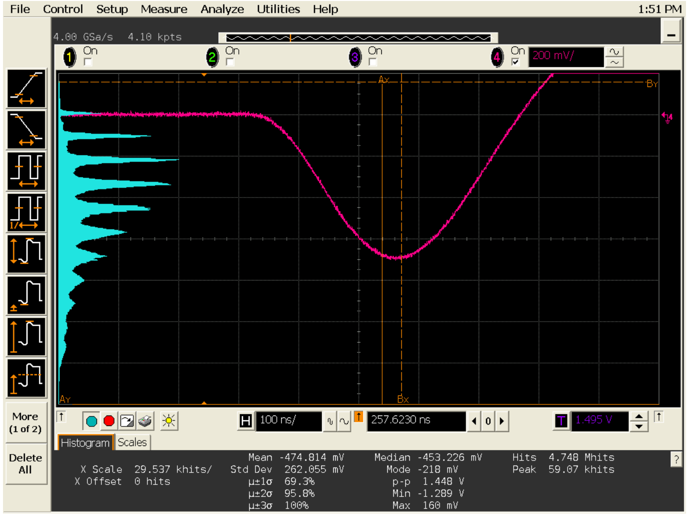

```
4.00 GSa/s   4.10 kpts
4 On ☑ 200 mV/
H 100 ns/   257.6230 ns   0   T 1.495 V

                        Mean -474.814 mV     Median -453.226 mV     Hits  4.748 Mhits
  X Scale  29.537 khits/  Std Dev  262.055 mV       Mode -218 mV       Peak  59.07 khits
 X Offset  0 hits           μ±1σ  69.3%             p-p  1.448 V
                            μ±2σ  95.8%             Min -1.289 V
                            μ±3σ  100%              Max  160 mV
```

Figure 13: Pulse with Projection Histogram

Copies of the two circuit diagrams for these pre-amps can be found in the appendix.

2.2.5 Comparison Circuit

The comparison circuit is a set of two analog devices, a discriminator and a comparator, which read voltage pulses from both pre-amps. Signals from the discriminator feed into the comparator and signals from the comparator feed out of this circuit into the oscilloscope. The circuit has two primary functions.

First, the Phillips Scientific discriminator only allows voltages above a tunable threshold through. The adjusted value for this threshold is set to 0.897 V. This function is important as it eliminates low voltage noise resulting not only from internal sources, but also from low energy ambient light which produces PE peaks below expected values for true scintillation events. This is discussed in more detail in section 3.12.

Second, the Phillips Scientific comparator outputs square wave logic pulse only when it recognizes a similar pulses from both pre-amps within a logic pulse window on the order of nanoseconds. This function results in a single square pulse out to the discriminator if the two occur in relative unison (within this logic pulse time). This is formally known as triggering on coincidence. Due to the much faster response rate of the SiPM, coincident pulses can adequately be accounted for with this device. As such, the response rate for the coincidence trigger is the primary analog constraint on response in data acquisition. This component can also be set to veto high energy pulses which might be caused by cosmic rays, but hasn't been employed in the experiment thus far due to its presumed negligible affect on the final data product.

The final data product from this section of the experiment is a single square wave logic pulse correspond to a scintillation event in the scintillator plate. This logic pulse is sent to an oscilloscope in order to obtain filtered, triggered data from the SiPMs directly.

2.2.6 Oscilloscope, DAQ, and Data Storage

The two signals out of the SiPM and the single signal from the comparison circuit are fed into a four channel digital oscilloscope before data acquisition. This is done as a visual check to ensure that pulse lengths and amplitudes from the two different SiPMs are in relative agreement and to convert the voltage readings into the scope to a digital data signal for storage on the DAQ. The oscilloscope can also output an averaged histogram over pulse events wherein PE peaks can be confirmed, enabling a second visual check on the data. Each coincident, filtered pulse from a single detection event is digitized and potentially sent to the DAQ via USB.

When the data acquisition channel is open, the terminal on the DAQ (which controls the widget program) monitors the data acquisition. After a number of events determined in the stepper code, the DAQ issues a command to the oscilloscope to cease data output (it closes the data acquisition channel) and commands the widget to move the source via the stepper motors. When the source is in its new position, the terminal opens the data acquisition channel. This process is automatically repeated until a determined number of coincidence events is saved per X and Y location of the source per SiPM.

This process results in a compact data product which contains digitized pulses. These pulses are categorized by location, SiPM, and by time of modification. A typical X and Y location folder contains the time that it was created and 1000 events, each with two pulses (one from each SiPM).

2.3 Stage Three: Data Analysis

The data analysis section contains no hardware. All of the code used to analyze the data gathered from the hardware side of the experiment is detailed here, along with an explanation of each stage and its purpose in the experiment as a whole.

2.3.1 Calibration

Before any reliable data can be taken for the experiment, the capability of the apparatus must first be tested. Calibration data serves this purpose. In order to obtain said data, an LED is attached via a multiclad WLS fiber to each SiPM individually. This LED outputs light at determinable intensities, simulating events from the scintillator at discrete PE peaks. This data is accumulated over 10000 events via the above process and saved to a single position folder.

This calibration data is then run through calibration code which fits the data and returns a set of important parameters for the analyzer function described in section 2.3. These parameters are the average, the gain, the pedestal, the norm, the standard deviation, and the square of the standard deviation. With these parameters fixed in the analyzer code for each SiPM, two essentially coupled consequences follow. First, if the apparatus cannot adequately map detection events resulting in PE response from the SiPM, the fit function will not fit the data properly. This is a check on the aptitude of the apparatus as a whole. Second, the analyzer function cannot operate without this essential information correlating PE peaks to pulse data from each SiPM. Without this calibration data, the PE peaks that the function seeks to fit will not lie in the ranges that it is looking in, and the final analyzed product will not be useful. Figure 14 depicts a typical calibration histogram with fits which will now be discussed.

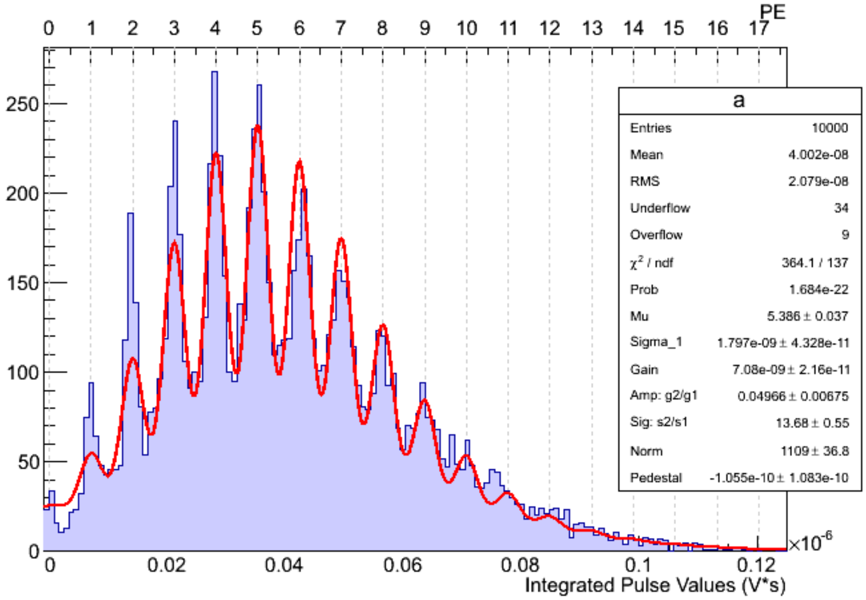

Figure 14: Calibration Histogram with Fitted PE Peaks

2.3.2 Analysis Function

Perhaps the most important part of the experiment is the analyzer program written by Shawn Beckman and edited by Professor Jamie Nagle and Sebastian Seeds. This program is used primarily to give PE yields per location of the source over the scintillator and to bin these to a histogram. The final data product from data acquisition, and the input to the analyzer function, is a large set of pulses which range between a static minimum amplitude set by the discriminator, and a dynamic maximum amplitude which is set by event detection from the SiPM. The amplitude of each pulse roughly corresponds to the photons incident to the SiPM which is correlated to the energy deposited in the WLS fiber. More precisely, the integral of the pulse corresponds to the PE from the SiPM. To obtain this value, an inverted Gaussian is fitted to the raw pulse data, and the area between the curve and the 0 V axis is calculated. This represents the essential data product for later analysis. Figure 15 shows a grouping of four such event pulses with the Gaussian fits necessary for integration. Each event returns a single integrated pulse value for the later histograms.

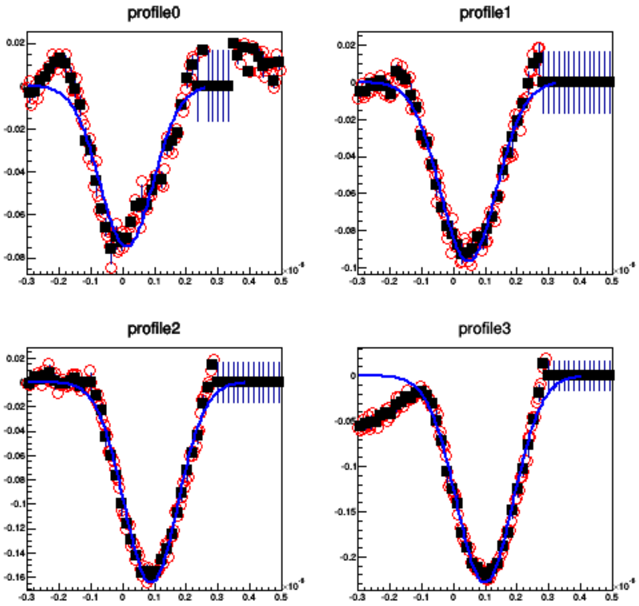

Figure 15: Four Event Pulses with Gaussian Fits

This said, the actual integrated pulse data does not exactly come in discrete levels corresponding to PEs. Instead it comes as a large scale Poisson distribution around the average energy deposited at each location modulated with smaller scale Gaussian distributions around PE peaks from the each SiPM. As a result it is necessary to analyze a distribution of these integrated pulse values. Two types of fits will be necessary for this analysis. The first, Poisson fitting, will be used to provide an overall structure for the distribution. The second, Gaussian fitting, will be modulated into the Poisson fitter in order to capture the finer PE structure.

Poisson fitting is the process by which a Poisson distribution function is modeled over a distribution. Here, the distribution is a histogram of integrated pulse values versus events. This distribution represents an entire set of data for a position such that the counts represented sum to the number of determined events per location. Poisson distributions are typically used for low statistics and for distributions which aren't symmetric about the mean, and is generally given by:

$$P\left(x\right)=\frac{e^{-\lambda}\lambda^{x}}{x!}$$

Here λ is the expected value of the variable and its variance. Due to the function of the discriminator, much of the lower integrated pulse data is cut out of the final data product and the distribution rises quickly from zero. As a result of this and that the distributions here are counting distributions, the overall distribution of the integrated pulse data is best modeled with a Poisson curve whose parameters are set by calibration data.

This doesn't capture the entire structure of the data, however. A peak at each discrete PE count from the SiPM should also be evident, which a Poisson fit alone will not account for. In order to get the peaks along the Poisson curve, a series of spaced Gaussian curves must be modulated into the fit. Gaussian distributions are the large statistical limit of the Poisson curve, and is given by:

$$P(x) = \frac{1}{\sigma\sqrt{2\pi}} e^{-(x-\mu)^2 / 2\sigma^2}$$

Here μ is the mean value of the distribution, σ is the standard deviation, and σ^2 is the variance. Functionally, this means that the separately spaced Gaussian fits will be symmetric about a mean location positioned at each PE peak as defined by the calibration parameters. Figure 16 depicts one such distribution and fit. This piece is necessary in order to obtain a value for the mean integrated pulses per location which corresponds to a PE count. Without it, the mean might be distorted by low statistics and pulled away from the truer value by the Poisson fit.

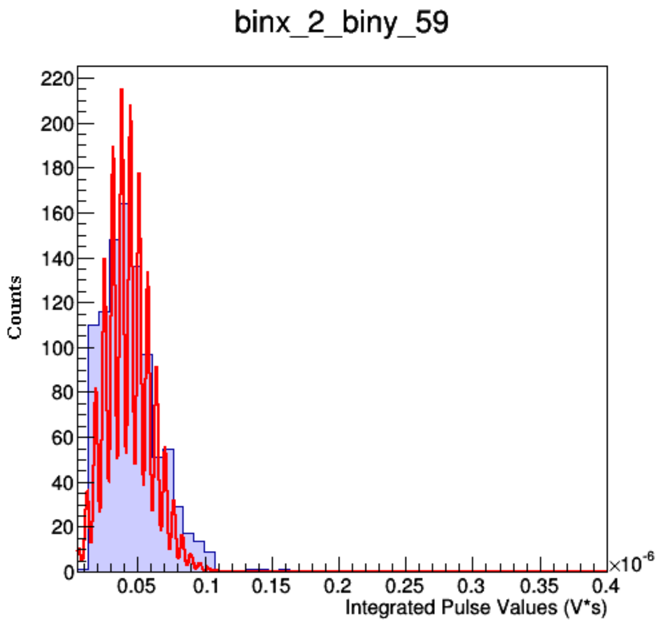

Figure 16: Event Histogram with Fitted PE Peaks

Both of these fit functions operate by minimizing the chi-square of a distribution. This essentially takes the error of the input histogram and creates a model curve which minimizes the variance. In this way, the error after the fit function is from the fit function itself. Each fit reports a set of error parameters which correspond to the efficacy of curve to fit the data.

With a mean integrated pulse fit value which corresponds to a PE count, a value can be asserted for the PEs generated at the SiPM at a given location X and Y. The final function of the the analyzer code is to take this value, properly calibrated to PE counts, and bin it to a histogram. By looping over this process many times, a two dimensional histogram can be rendered where the structure of the scintillation event response across a sample scintillator is clear to see. Figure 17 is an example of an earlier success of this process.

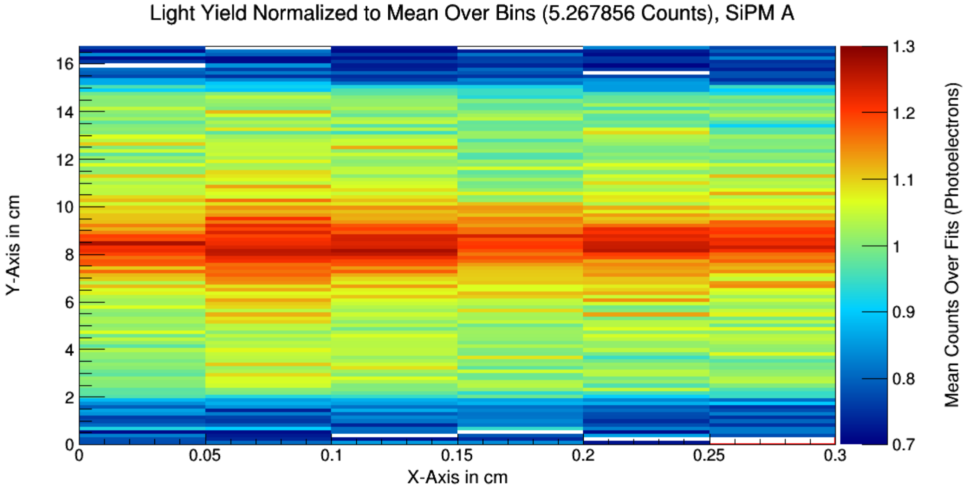

Figure 17: Example Scan Histogram with Six Passes over Panel with Fiber in Middle

In addition to creating a histogram modeling the PE response across a scintillator panel, the analysis code also reads in the time of last modification per location data file. The difference between this value and the next is binned to a histogram over the same geometry as the response histogram, enabling an analysis of the time it takes to obtain coincidence pulses per location. Section 3.1 deals with this data.

The analysis procedure isn't complete. Additional code can shape the output histograms to be more quantitative and other important parameters in the data can be analyzed.

2.3.3 Basic Interpreter

The interpretation code was written by Sebastian Seeds in order to emphasize certain features of the histograms created by the analyzer code and to compare different runs against each other. The first stage of the interpreter code sets appropriate parameters to the axes of the histogram and establishes a color scheme suitable to interpretation. It also creates projection histograms for scintillator layout which have symmetry along X or Y. The data presented in this thesis fits this description. Such a one dimensional histogram gives a quantitative response across a scintillator in one direction. Refer to section 3.1 for analysis of these histograms.

The second stage of the interpreter compares three histograms against one another, and allows for simultaneous plots. This comparison enables trend analysis and relative variance analysis. Both are important for the conclusions drawn here.

Input histograms can be altered in both interpreter macros to suit the particulars of the data set, such as analysis parameters and exploited symmetries.

2.3.4 Temperature Monitor

The temperature monitor software is proprietary and employed on a separate computer other than the DAQ. It is attached to a thermistor which enables temperature readings accurate to 0.06° C [12]. This thermistor is placed in the light insulating box and data is continuously taken from it. Refer to 2.42 for a description of the thermistor used. A broad histogram for temperature versus time is available for comparison against PE response from the software. Exact correlation has not been performed. Refer to section 3.13 for analysis of temperature for this experiment.

2.4 Ancillary Hardware

All additional hardware not included in the processing of the essential data package is included in this subsection. It includes a vacuum chamber for preparing scintillators for testing and a thermistor for gathering temperature data in the light insulating box.

2.4.1 Vacuum Chamber

An important parameter tested in this experiment is the relative light coupling capacity of epoxy and optical grease. In order to obtain the highest possible optical coupling from epoxy, the air bubbles present in the liquid phase of the resin must be removed. A vacuum chamber was employed for this purpose. This vacuum was effective to about 1 torr, and visually removed the bubbles present in the epoxy. Figure 18 shows this vacuum chamber.

Figure 18: Shot of Vacuum Chamber

The vacuum chamber itself was machined from two pieces of lucite. The first piece was machined such that a chamber was bored out of a central region. A single shaft was milled out of one side of this chamber. On the exposed top of the chamber foam tape was glued to prevent air loss after pumping. An airtight nozzle was affixed to the milled shaft on the outside of the chamber. In operation, the second piece of lucite is simply laid on the top of the apparatus, and the air is pumped out.

2.4.2 Thermistor

In order to take temperature readings for comparison against PE response data, a thermistor was used. A thermistor is a resistor whose internal resistance changes relatively greatly and linearly with temperature. This relationship is given by:

$$\Delta R = k\Delta T$$

This enables the correlation of temperature to a voltage reading when after a current is passed through it. The HID USB thermistor is connected to the secondary computer via USB. which allows for temperature readings to be taken from inside the light insulating box.

3 Data and Results

3.1 Apparatus and Analysis

The primary results of the experiment thus far are hardware and software related. Where the overarching interest of the research here is to find a reproducible way to equalize PE response across a scintillator, a functional apparatus to test this response is essential. To this end, much of the success of the experiment thus far has been in the creation and maintenance of the hardware and software comprising the apparatus. There are several independent pieces of confirming evidence for this success. This said, the analyzed results of the experiment are promising, and point towards a solution for the problem of equalizing light yield detailed above.

3.1.1 Fiber Geometry and Photoelectron Response

Foremost among the confirming evidence is the consistency of the results from similar scintillator plates over several trials. Figures 19 and 20 illustrates several tests over the same scintillator.

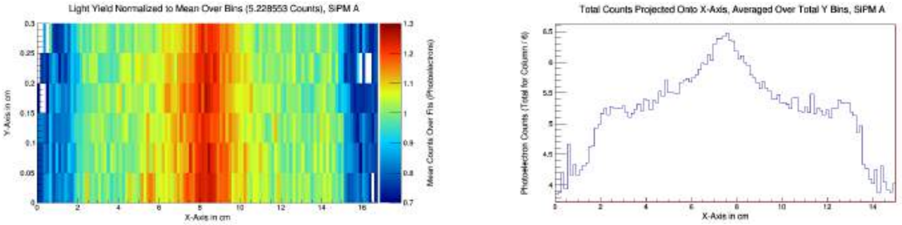

(a) Six Pass Scan Histogram

(b) Mean Count X-axis Projection

Figure 19: Z Scan from a Wrapped Panel

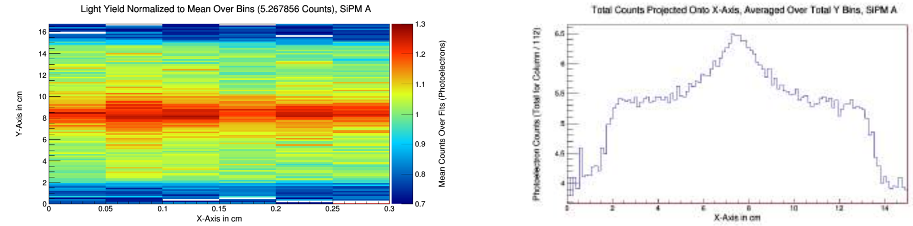

(a) Six Pass Scan Histogram

(b) Mean Count X-axis Projection

Figure 20: N Scan from the Same Wrapped Panel

The consistency of these results shows the efficacy of the apparatus. Each of the six shown scan histograms (and many others not included here) display all the crucial features expected from test runs with a single straight fiber. The edge of the scintillator corresponds to the relatively low PE means indicated by the cool colors at the ends. The WLS fiber corresponds to the relatively high PE means indicated by the hotter colors in the middle of the scan histogram. This result is consistent with a functional analyzer function interpreting event data derived from controlled fluorescence events.

Beyond visual confirmation, the integrated pulse values for each location on the scan histogram can be compared. This analysis yields further evidence that the apparatus is operating effectively as the mean for each location histogram can be checked against the fit function. Fits which do not correspond to the mean value of the event distributions there have been observed to yield extreme values easily distinguished on the scan histogram.

Null scans have also been performed. This kind of scan is the result of several bins filled with 1000 events where the source is prevented from moving over the scintillator by the stepper code. These scans yield uniform results consistent with the PE yields observed in control scan histograms when the source is not over the scintillator. This result further shows that the analyzer function is interpreting meaningful data.

The length of time that each location takes to fill 1000 events has also been analyzed. This sampling delay has been quantified for a known scan and plotted on a histogram. Figure 21 illustrates this comparison. The results of this comparison show that the low PE means interpreted an absence of fluorescence events from the source correspond to lower sampling rates. This is expected because the radioactive source provides a high rate of electrons incident to the scintillator for fluorescence events to occur. The absence of such a consistent source of electrons should correlate to slower sampling rates, and does.

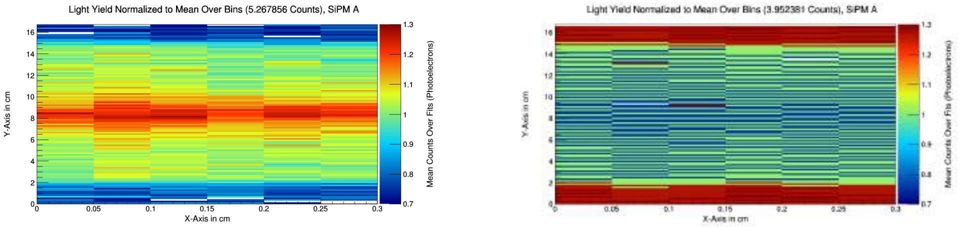

(a) Six Pass Scan Histogram

(b) Sampling Time Per Location

Figure 21: N Scan from the Same Wrapped Panel

Finally, the temperature within the light insulating box has been controlled and monitored. The results from this attention have put the mean variance from the mean of 23° C at ±1.5° C clustered around 23°. This is within the operational limits of both the SiPM and the scintillator, both of which see varying response as a function of larger temperature differentials. No correlation between PE response and temperature has been necessary due to consistency among mean PE response over many scans.

3.1.2 Fitting and Photoelectron Peaks

The most promising results of the experiment for the sPHENIX upgrade are in the functional fits added to the histograms. Figure 22 illustrates one such fit, but many others follow a similar pattern.

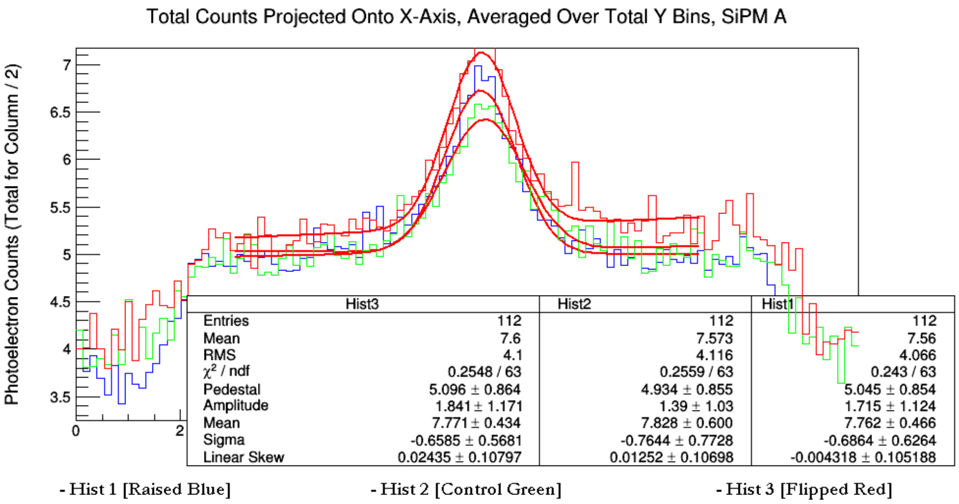

Figure 22: Three Projection Comparison

Topically, these fits show a mean 20% increase in PE response corresponding to positions of the source above the WLS fiber. More importantly, though, these fits show that the functional dependence of PE yield on distance from an optical fiber in a scintillator drops exponentially and plateaus at a constant value. While these fits are not, in general, indicative of the PE response from more elaborate fiber geometries, they are telling. Efforts to expand these results to larger scintillators are underway and, if consistent, might provide a method for equalizing response across the scintillator. Figure 23 show preliminary results from such a test.

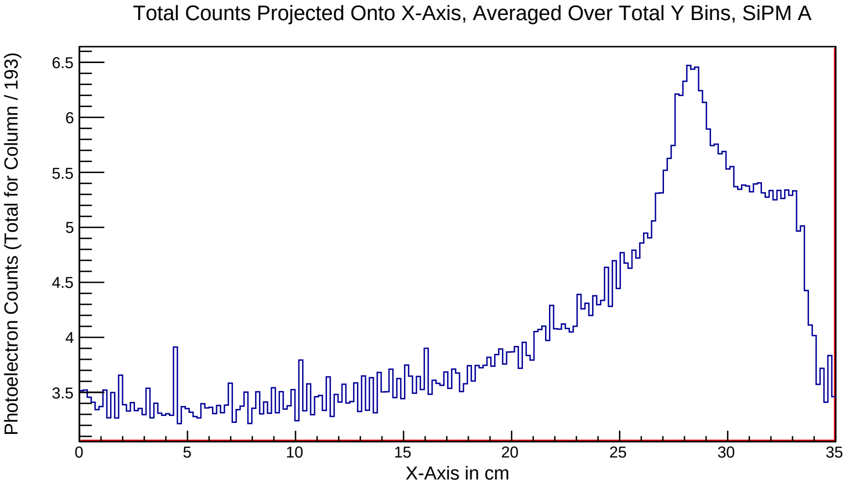

Figure 23: Projection Histogram for End-Fiber Geometry

If these fits can be generalized to scintillators as large as those used in the HCAL at PHENIX, then it should be possible to equalize PE yield by utilizing an end-fiber geometry and vetoing on coincidence with another small scintillator. This second scintillator might be positioned between the area of greater effect of the first scintillator and the event chamber.

While the preliminary tests show that this won't be simple, increasing reflectivity on the edges of the panel might keep total internal reflection high enough to see a plateau across even the larger panel. The results of the ongoing tests should indicate if this strategy, or something like it, might prove beneficial.

3.1.3 Secondary Tests

In an effort to improve the resolution of PE peaks in event histograms, an overall increase in light yield at each SiPM was desired. Pursuant to this, a single panel was prepared with a WLS fiber epoxied into its groove with optical epoxy. This was done with a vacuum chamber such that the air in the epoxy was removed from the resin during its liquid phase. The result of this effort was a mean increase in light yield of 0.5 PEs, and a similar lack of clear PE peaks in event histograms. Figure 22 shows comparative results which yield this result.

Optimally, the behavior of the calibration event histogram (with clear PE peaks) should be evident over a shorter and longer Poisson distribution for each event histogram. Epoxy has not provided any insight as it lacks the ability to increase light yield significantly. The cause of this discrepancy is still being investigated. This being said, these results indicate that efforts to simply increase light yield significantly should not pursue epoxy due to marginal benefits and higher cost.

In an effort to explain the rapid increase in PE response when the source is positioned above the WLS fiber, a test of the comparative PE responses between two orientations of the scintillator was performed. The results of this comparison can be observed in figure 22.

These histograms indicate a similar functional dependence of PE yield as the other scans. This supports the conclusion that the observed increase in PE response next to the fiber is due to more captured fluorescence from the scintillator. While these data aren't conclusive, they do indicate that the sudden increase in PE response evident across the scintillator is ultimately due to fluorescence from the scintillator and not from fluorescence from the WLS fiber directly.

Separately, the variance from the fit for event histogram projections shows a marked increase for those corresponding to orientations of the scintillator where its milled groove holding its corresponding WLS fiber is facing the source. This is consistent with the explanation that fluorescence from source electrons which enter the fiber directly result in higher PE yield, but do so inconsistently. This is an intermediary conclusion, but a valuable one for future research.

3.2 Future Projections

There is much left to do with the apparatus. Foremost, testing on the end-fiber geometry mentioned above will continue. The results of this research may well accomplish the primary motivation for this research. Investigation into this subject will likely take the project into 2015.

Over this period and following it, two additional inquiries will be important. First, clear PE peaks can be made evident in event histograms. Towards this end, increased statistics and better binning resolution in event histograms will be pursued. With this lack of PE peaks explained and corrected, each scan histogram projection should see a smaller variance from a Gaussian fit and further confirm the results stated above. Second, area of affect data will be collected for electrons which leave the lower aperture of the source collimator and enter the scintillator. Where this area can be minimized, greater resolution in scan histograms can ultimately be obtained. Consistent with this, better fits to scan histograms are also possible.

Depending upon the results of this research, investigation into the efficacy of light absorbing and reflecting materials coupled to the scintillator for the purpose of equalizing light yield can also be pursued. Such research might entail the application of paint or thin coupled reflective material around the scintillator. Further, more elaborate fiber geometries can also be investigated.

3.3 Conclusions

The apparatus built and maintained for this experiment has much to offer the HCAL in the sPHENIX upgrade. With meaningful data, the hardware and software of this project has already proven itself to be effective towards modeling photoelectron yield in scintillating plates coupled to silicon photomultipliers. To the extent that this kind of setup is important for the sPHENIX upgrade, the functional apparatus used in this experiment will continue to bear fruit.

The results of several months of tests with the apparatus are promising. Where consistent results indicate that photoelectron response plateaus for simple fiber geometries, some simple measures can be applied to correct for the mean 20% differential in photoelectron response across scintillators which use wavelength shifting fibers. Efforts to test this theory are underway.

With a more accurate hadronic calorimeter installed in the PHENIX detector, results of heavy ion collisions analyzed from there can only improve. As such, the efforts made on this project and detailed in this thesis have been toward raising the overall efficacy of research into the quark-gluon plasma.

Appendices

A Circuit Diagram

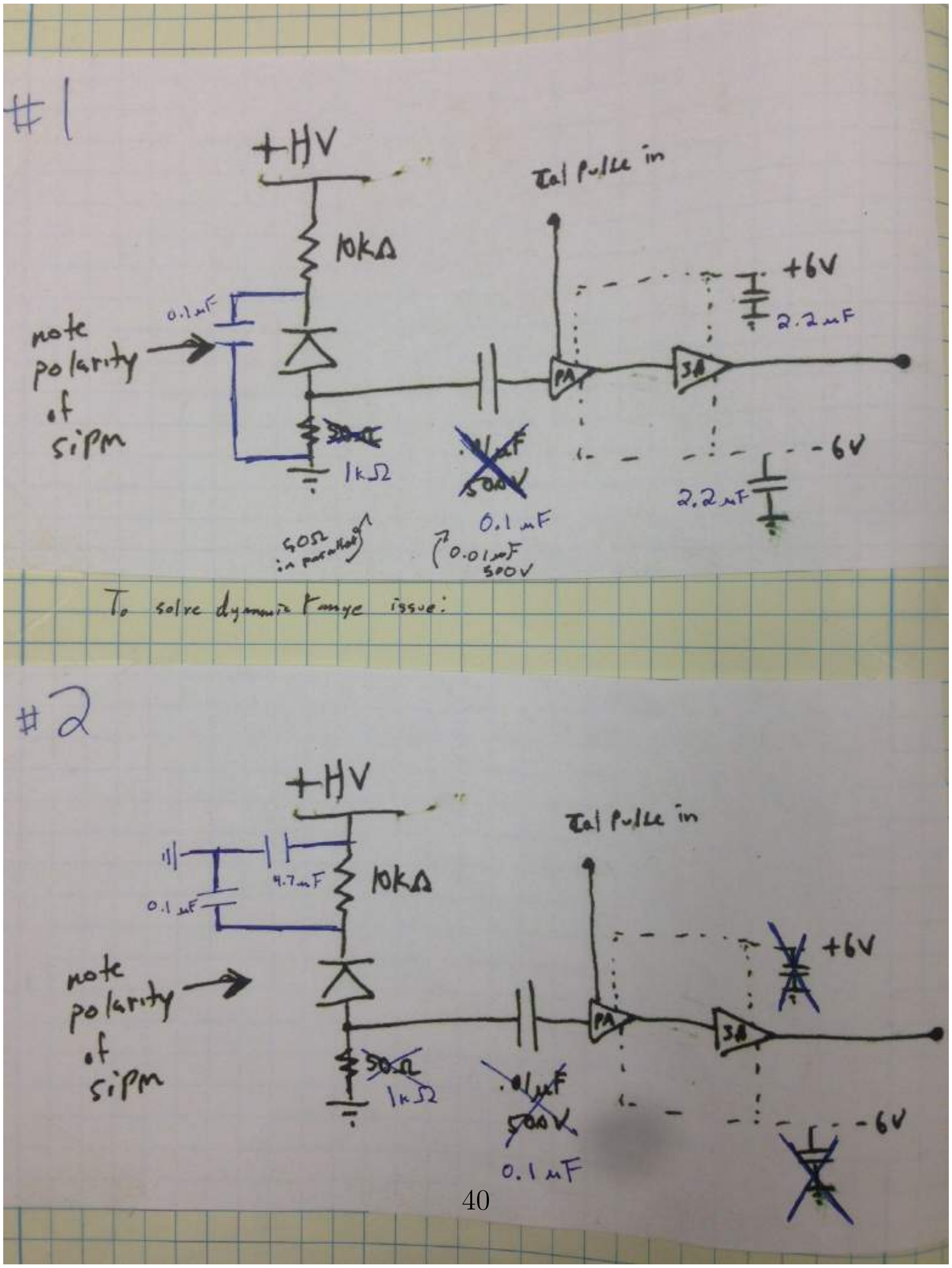

Figure 24: Circuit Diagram for Pre-amps

References

[1] Scintillating Optical Fibers, 2005.

[2] C Aidala, NN Ajitanand, and Y Akiba. sPHENIX: An Upgrade Concept from the PHENIX Collaboration. *arXiv preprint arXiv: . . .*, 2012.

[3] E.V. Akhrameev, L.B. Bezrukov, I.M. Dzaparova, I.Sh. Davitashvili, T. Enqvist, H. Fynbo, Zh.Sh. Guliev, L.V. Inzhechik, a.O. Izmaylov, J. Joutsenvaara, M.M. Khabibullin, a.N. Khotjantsev, Yu.G. Kudenko, P. Kuusiniemi, B.K. Lubsandorzhiev, O.V. Mineev, L. Olanterä, V.B. Petkov, R.V. Poleshuk, T. Räihä, B.a.J. Shaibonov, J. Sarkamo, a.T. Shaykhiev, W. Trzaska, V.I. Volchenko, G.V. Volchenko, a.F. Yanin, and N.V. Yershov. Multi-pixel Geiger-mode avalanche photodiode and wavelength-shifting fibre-optics readout of plastic scintillator counters for the EMMA underground experiment. *Nuclear Instruments and Methods in Physics Research Section A: Accelerators, Spectrometers, Detectors and Associated Equipment*, 610(1):419–422, October 2009.

[4] Slide Assembly. Lead Screw Coupling : Steel. pages 2–6.

[5] D Beznosko. Novel Multi-pixel Silicon Photon Detectors and Applications in T2K. *arXiv preprint arXiv:0910.4429*, 2009.

[6] Great Britain and Pergrmon Prerr. REVIEW OF PROGRESS ON SClNTiLLATlON FLUORS FOR THE DETECTORS OF THE SSC JOEL M . KAUFFMAN Chemistry Department , Philadelphia College of Pharmacy & Science 909 South 43rd St ., Phila ., PA 191064495 ABSTRACT The limits of scintillation decay time (t) in. *Radiat. Phys. Chem.*, 41(112):365–371, 1993.

[7] Photomultiplier Design, Electron Optics, Photomultiplier Characteristics, and Photomultiplier Applications. Photomultiplier Handbook. pages 8–80.

[8] Chemical Identity and Radiological Properties. 4 . CHEMICAL , PHYSICAL , and RADIOLOGICAL INFORMATION Table 4-1 . Chemical Identity of Strontium and Strontium Compounds. pages 189–197, 1997.

[9] Hamamatsu Photonics K K. MPPC Multi-Pixel Photon Counter. (January), 2014.

[10] Glenn F. Knoll. *Radiation Detection and Measurement*. Danvers, MA, 4th edition, 2010.

[11] Kuraray. Kuraray-PSF-Y11.pdf.

[12] PCSensor. Thermistor Tech Specs.

[13] SPHENIX. jfrantz_cal_workshop_121410.

[14] A Vacheret and GJ Barker. Characterization and simulation of the response of Multi-Pixel Photon Counters to low light levels. *Nuclear Instruments and . . .*, 2011.